THE JOURNAL OF BIOLOGICAL CHEMISTRY VOL. 284, NO. 39, pp. 26941–26950, September 25, 2009

Detailed Mechanistic Insights into HIV-1 Sensitivity to Three Generations of Fusion Inhibitors*[S]

Received for publication, April 6, 2009, and in revised form, July 13, 2009 Published, JBC Papers in Press, July 17, 2009, DOI 10.1074/jbc.M109.004416

Dirk Eggink[‡], Johannes P. M. Langedijk[§], Alexandre M. J. J. Bonvin[¶1], Yiqun Deng[‖], Min Lu[‖], Ben Berkhout[‡], and Rogier W. Sanders[‡2]**

*From the [‡]Laboratory of Experimental Virology, Department of Medical Microbiology, Center for Infection and Immunity Amsterdam, Academic Medical Center of the University of Amsterdam, 1105 AZ Amsterdam, The Netherlands, [§]Pepscan Therapeutics BV, 8423 RC Lelystad, The Netherlands, the [¶]Bijvoet Center for Biomolecular Research, Science Faculty, Utrecht University, 3584 CH Utrecht, The Netherlands, and the [‖]Department of Biochemistry and **Department of Microbiology and Immunology, Weill Medical College of Cornell University, New York, New York 10021*

Peptides based on the second heptad repeat (HR2) of viral class I fusion proteins are effective inhibitors of virus entry. One such fusion inhibitor has been approved for treatment of human immunodeficiency virus-1 (T20, enfuvirtide). Resistance to T20 usually maps to the peptide binding site in HR1. To better understand fusion inhibitor potency and resistance, we combined virological, computational, and biophysical experiments with comprehensive mutational analyses and tested resistance to T20 and second and third generation inhibitors (T1249 and T2635). We found that most amino acid substitutions caused resistance to the first generation peptide T20. Only charged amino acids caused resistance to T1249, and none caused resistance to T2635. Depending on the drug, we can distinguish four mechanisms of drug resistance: reduced contact, steric obstruction, electrostatic repulsion, and electrostatic attraction. Implications for the design of novel antiviral peptide inhibitors are discussed.

The HIV-1 envelope glycoprotein complex (Env),[3] a class I viral fusion protein, is responsible for viral attachment to $CD4^+$ target T cells and subsequent fusion of viral and cellular membranes resulting in release of the viral core in the cell. Other examples of viruses using class I fusion proteins are *Coronaviridae* (severe acute respiratory syndrome virus), *Paramyxoviridae* (Newcastle disease virus, human respiratory syncytial virus, Nipah virus, Hendra virus), and *Orthomyxoviridae* (influenza virus), some of which cause fatal diseases in humans (1–3). The entry process of these viruses is an attractive target for therapeutic intervention.

The functional trimeric Env spike on HIV-1 virions consists of three gp120 and three gp41 molecules that are the products of cleavage of the precursor gp160 by cellular proteases such as furin (4, 5). The gp120 surface subunits are responsible for binding to the cellular receptors, whereas the gp41 subunits anchor the complex in the viral membrane and mediate the fusion of viral and cellular membranes. Env undergoes several conformational changes that culminate in membrane fusion. The gp120 subunit binds the CD4 receptor, resulting in creation and/or exposure of the binding site for a coreceptor, usually CCR5 or CXCR4 (6, 7). Two α-helical leucine zipper-like motifs, heptad repeat 1 (HR1) and heptad repeat 2 (HR2), located in the extracellular part of gp41, play a major role in the following conformational changes. Binding of the receptors to gp120 induces formation of the pre-hairpin intermediate of gp41 in which HR1 is exposed and the N-terminal fusion peptide is inserted into the target cell membrane (1, 8–12). Subsequently, three HR1 and three HR2 domains assemble into a highly stable six-helix bundle structure that juxtaposes the viral and cellular membranes for the membrane merger. Other viruses with class I viral fusion proteins use similar HR1-HR2-mediated membrane fusion for target cell entry.

Peptides based on the HR domains of class I viral fusion proteins have proven to be efficient inhibitors of virus entry for a broad range of viruses (13–17). The HIV-1 fusion inhibitor T20 (enfuvirtide (Fuzeon)) has been approved for clinical use. T20 mimics HR2 and can bind to HR1, thereby preventing the formation of the six-helix bundle (Fig. 1) (18–21). T1249 is a second-generation fusion inhibitor with improved antiviral potency compared with the first-generation peptide T20 (22–25). Recently, a series of more potent third-generation fusion inhibitors were designed (26, 27). These include T2635, which has an improved helical structure that increases stability and activity against both wild type (WT) HIV-1 and fusion inhibitor resistant variants.

Both the *in vitro* and *in vivo* selection of resistance has been described for T20 (28–33) and T1249 (23, 34–36). Resistance is often caused by mutations in the HR1 binding site of the fusion inhibitor. In particular, substitutions at positions 36 (G36D/M/S), 38 (V38A/W/M/E), and 43 (N43D/K) of gp41 can cause resistance. Strikingly, substitutions at position 38 can cause resistance to both T20 and T1249, but distinct amino acid substitutions are required. At position 38 only charged amino acids

* This work was supported in part by National Institutes of Health Grant AI42382 (to M. L.). This work was also supported in part by AIDS Fund (Amsterdam) Grant 2005021 (to B. B.).

[S] The on-line version of this article (available at http://www.jbc.org) contains supplemental Figs. S1–S3 and Table S1.

[1] Supported by a Vici grant from the Netherlands Organization for Scientific Research.

[2] Recipient of an Anton Meelmeijer fellowship, a Veni fellowship from the Netherlands Organization for Scientific Research-Chemical Sciences, and an amfAR Mathilde Krim research fellowship. To whom correspondence should be addressed: Laboratory of Experimental Virology, Dept. of Medical Microbiology, CINIMA, Academic Medical Center of the University of Amsterdam, Meibergdreef 15, 1105 AZ Amsterdam, the Netherlands. Tel.: 31-20-5665279; Fax: 31-20-6916531; E-mail: r.w.sanders@amc.uva.nl.

[3] The abbreviations used are: Env, envelope glycoprotein complex; HIV-1, human immunodeficiency virus type 1; HR, heptad repeat; WT, wild type.

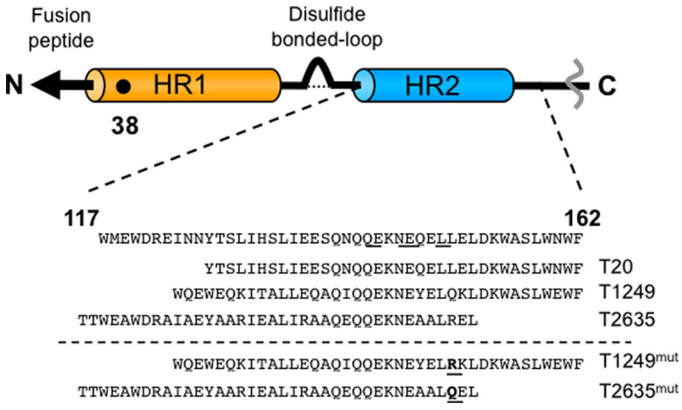

FIGURE 1. **Schematic of the gp41 ectodomain.** HR1 and HR2 are represented as *cylinders*, and position 38 in HR1 is indicated. Residues Gln-142, Asn-145, Glu-146, and Leu-149, which interact with residue 38, are *underlined* in the HR2 sequence. HR2-based peptide fusion inhibitors are shown *underneath*. Mutations introduced in T1249^{mut} and T2635^{mut} are *bold* and *underlined*. Numbering is based on the sequence of HXB2 gp41.

(V38E/R/K) cause resistance to T1249 (35). Surprisingly, none of the known T20 and T1249 resistance mutations at position 38 affect the susceptibility to the third generation inhibitor T2635.

We hypothesized that the use of HIV-1 as a model system could provide a more detailed understanding of resistance to fusion inhibitors. We, therefore, analyzed the effect of all 20 amino acids at resistance hotspot 38 on Env function, viral fitness, biochemical properties of gp41, and resistance to the fusion inhibitors. From the results we can propose four resistance mechanisms that differ in the way the drug-target interaction is affected at the molecular level. Furthermore, we can deduce general principles on the mechanisms of resistance against fusion inhibitors and the requirements for effective antiviral drugs.

EXPERIMENTAL PROCEDURES

Peptide Synthesis—Peptides T20, T1249, and T2635 were synthesized as described previously (35). A more detailed description of the procedure is given in the supplemental material.

Construction of HIV-1$_{LAI}$ Molecular Clones—The full-length molecular clone of HIV-1$_{LAI}$ (pLAI) (37) was used to produce WT and mutant viruses. The plasmid pRS1 was used to introduce mutations at position 38 as described previously (35, 38), and the entire *env* gene was verified by DNA sequencing. Mutant *env* genes in pRS1 were cloned back into pLAI as SalI-BamHI fragments. Each virus variant was transiently transfected in C33A cells by calcium phosphate precipitation as previously described (39). The virus-containing supernatant was harvested 3 days post-transfection, filtered, and stored at −80 °C, and the virus concentration was quantitated by capsid CA-p24 enzyme-linked immunosorbent assay as described previously (40).

IC$_{50}$ and Infectivity Determination—The TZM-bl reporter cell line (32, 41) stably expresses high levels of CD4 and HIV-1 co-receptors CCR5 and CXCR4 and contains the luciferase and β-galactosidase genes under the control of the HIV-1 long-terminal-repeat promoter. The TZM-bl cell line was obtained through the NIH AIDS Research and Reference Reagent Program, Division of AIDS, NIAID, National Institutes of Health (John C. Kappes, Xiaoyun Wu, and Tranzyme Inc. (Durham, NC)). Single-cycle infection experiments and inhibition experiments using TZM-bl cells were performed as described (35). A more detailed description of the procedure is given in the supplemental material.

We note that some differences in relative infectivity were found compared with our previous studies (35). Similar small inconsistencies compared with our previous studies were observed with the biophysical experiments. We can attribute these differences to the different Env background in which the substitutions were introduced. We used the HIV-1$_{LAI}$ sequence here, whereas a N125S mutation was present in the earlier studies to mimic the HR2 sequence from the patient isolate we studied (33, 35). The exact consequences of this substitution for virus infectivity and gp41 function in general are currently under investigation.

Homology Modeling—The structures of the HIV-1, strain LAI, HR1 trimer in complex with an inhibitory peptide was based on homology modeling using the x-ray structure of SIV gp41 six-helix bundle (PDB 2EZO and 1QCE), which is the most complete example of six-helix bundles in the data base, and it contains the largest part of the interaction site of the HR1 trimer with the HR2-based inhibitory peptides. Part of the HR2 helix was used as a model for T20, T1249, and T2635. In case of T2635, the helix corresponding to HR2 was extended with seven residues. Model building was performed using the automated protein-modeling software on the SWISSMODEL protein-modeling server (42, 43). Model quality was verified using WhatCheck (44).

Binding Energy Calculations—To get an estimate of the binding energy of the various mutants, the models of the various inhibitory peptides and their mutants were subjected to a gentle refinement in explicit solvent (8 Å water shell) using HADDOCK2.0 (45, 46). For this, randomization of starting orientations and rigid-body energy minimization were turned off, and only the final water refinement stage was performed consisting of a heating phase (100 molecular dynamics (MD) steps at 100, 200, and 300 K), a sampling phase (1250 MD steps at 300 K), and a final cooling phase (500 MD steps at 300, 200, and 100 K). Non-bonded interactions were calculated with the optimized potentials for liquid stimulations force field (47) using a cutoff of 8.5 Å. The electrostatic potential (E_{elec}) was calculated by using a shift function, whereas a switching function (between 6.5 and 8.5 Å) was used to define the van der Waals potential (E_{vdw}). The binding energy was approximated by the average HADDOCK score of the best four models after water refinement. The HADDOCK score consists of a weighted sum of intermolecular non-bonded energies and an empirical desolvation term (48): HADDOCK score = $1.0 \times E_{vdw} + 0.2 \times E_{elec} + 1.0 \times E_{desolv}$. We should remark that the binding energies we are referring to are estimates based only on the intermolecular electrostatic and van der Waals energies with an additional empirical desolvation term. They clearly should not be interpreted in terms of free energies and do not account for any entropic effects (except for the desolvation term that implicitly accounts for the solvent entropy gain upon binding). From all the calculated terms, the HADDOCK score was the one giving

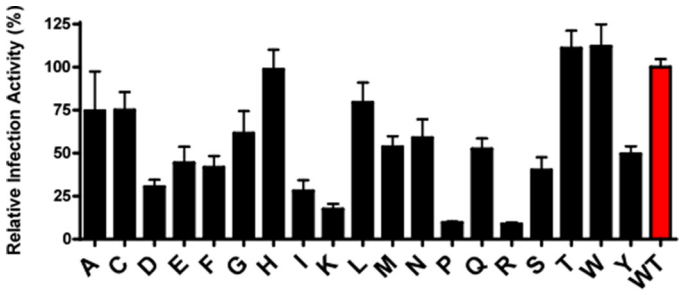

FIGURE 2. **Functional characterization of WT and 38 variants.** Single cycle infection assays in TZM-bl cells were performed with WT HIV-1_{LAI} (Val-38) and 19 variants with a substitution at position 38. The luciferase activity of infections performed in 4-fold was measured and corrected for background luciferase activity. The luciferase activity of WT was set at 100%, and the relative infectivities of the 38 variants were normalized accordingly.

the best correlation with the experimental data (data not shown).

Peptide Expression and Purification—The recombinant N36(L6)C34 model peptide and its variants were expressed in the *Escherichia coli* strain BL21(DE3)/pLysS by a modified pET3a vector (Novagen, San Diego, CA) and purified as described (35, 49, 50). The sequence of N36(L6)C34 is SGIVQQQNNLLRAIEAQQHLLQLTVWGIKQLQARILSGGRGGWMEWDREINNYTSLIHSLIEESQNQQEKNEQELL (with the six-residue linker underlined). Substitutions were introduced into the pN36/34 plasmid by the method of Kunkel (51) and were verified by DNA sequencing. Peptide identities were confirmed by electrospray mass spectrometry (Voyager Elite; PerSeptive Biosystems, Framingham, MA). Protein concentrations were determined by the method of Edelhoch (52).

Biophysical Analysis—Circular dichroism (CD) experiments were performed on an 62A/DS (Aviv Associates, Lakewood, NJ) spectropolarimeter equipped with a thermoelectric temperature control at 10 μM peptide concentration in phosphate-buffered saline as described (35, 49, 50). An ellipticity value at 222 nm ($[\theta]_{222}$) value of $-33{,}000$ degrees cm^2 dmol^{-1} was taken to correspond to 100% helix (53). Thermal stability was determined by monitoring $[\theta]_{222}$ as a function of temperature as described. All melts were reversible. Temperatures of midpoint unfolding transitions (T_m) were estimated by evaluating the maximum of the first derivative of $[\theta]_{222}$ in relation to the temperature data (54). Equilibrium ultracentrifugation measurements were carried out on an XL-A analytical ultracentrifuge equipped with an An-60 Ti rotor (Beckman Coulter, Fullerton, CA) at 20 °C as described previously (55) (35, 49, 50). Solvent density and protein partial specific volume were calculated according to solvent and protein composition, respectively (56). The apparent molecular masses of all N36(L6)C34 variants were within 10% of that calculated for an ideal trimer, with no systematic deviation of the residuals.

RESULTS

Virus Infectivity—We generated a set of 20 viruses based on the CXCR4-using HIV-1_{LAI} strain, each with a different amino acid at position 38 in gp41. To compare the infectivity of these viruses, we performed single cycle infection assays. Luciferase activity in TZM-bl reporter cells was measured 2 days post-infection (Fig. 2). Mutant viruses V38H/T/W revealed infectivity close to WT, but all other viruses showed decreased infectivity compared with WT, and some substitutions severely reduced infectivity (V38K/P/R). The lower infectivity of these viruses may be explained by a reduced efficiency of six-helix bundle formation because of an altered HR1-HR2 interaction (see below). In addition, substitutions at position 38 may have effects on protein folding or on subsequent conformational changes. The relatively dramatic impact of changes at position 38 on infectivity may explain the high level of conservation of this residue (Los Alamos data base; www.hiv.lanl.gov) (57).

Sensitivity to Fusion Inhibitors—Next, we investigated the susceptibility of our panel of viruses to the three generations of peptide inhibitors, T20 (first generation), T1249 (second generation), and T2635 (third generation), and determined their respective 50% inhibitory concentrations (IC_{50}) (Table 1, supplemental Fig. 1). These three inhibitors are based on the HR2 sequence or are derivatives thereof, and position 38 is part of the predicted binding site of all three inhibitors (see Fig. 1 and Fig. 5, *A–C*). Consistent with this, almost every substitution at position 38 caused high resistance to T20, except for the V38I and V38L substitutions. All other substitutions caused resistance to T20 ranging from 7.4-fold (V38M) to >200-fold (V38D/E/P). Resistance to T1249 was only observed with five amino acids (V38D/E/K/P/R; >4-fold resistance compared with WT), whereas other substitutions did not alter sensitivity to T1249 significantly. Interestingly, all charged amino acids caused resistance to T1249, the negatively charged amino acids (V38D/E) causing the highest resistance (28.8- and 34.1-fold). Despite the location within the predicted binding site for T2635, none of the substitutions at position 38 conferred significant resistance to the third generation peptide. It may be surprising that most variants are resistant to T20, because only a limited number of these (V38A/M/W) are frequently observed in different *in vitro* and *in vivo* settings. However, all previous studies are based on virus evolution, either in cell culture or in patients, which means that the likelihood of the underlying mutation favors certain escape routes. In an evolutionary setting, the virus will try to find a balance between resistance, viral fitness, and the ease of emergence of the codon change required for escape.

Biophysical Properties—To obtain mechanistic insight into the role of HR1 position 38 in fusion and resistance to fusion inhibitors, we studied the biophysical properties of the six-helix bundle. Analyzing the effects of substitutions at position 38 may provide explanations for differences in infectivity as six-helix bundle formation is an essential step during fusion. Furthermore, it can teach us about the resistance to fusion inhibitors as the interaction of these drugs with HR1 is comparable with the interaction of HR2 with HR1.

We introduced all 20 amino acids at position 38 in the recombinant HIV-1_{LAI} N34(L6)C28 peptide, which represents the six-helix bundle (49, 58), and compared their biophysical properties. Sedimentation equilibrium analysis showed that the molecular weights of the 20 six-helix bundle variants were all close to those calculated for the ideal trimer, indicating that all variants formed trimers (Table 2). CD was used to determine the extent of α-helical structure of the six-helix bundle variants. The WT peptide is ~100% α-helical, as indicated by the typical

TABLE 1

Resistance in single cycle infection assays

Values, presented in ng/ml, were calculated as described under "Experimental Procedures." Results are derived from experiments performed in duplicate, representative for at least three independent experiments. Inhibition curves of single cycle infection experiments can be found in supplemental Fig. S1.

Variant	T20		T1249		T2635	
	IC_{50} (S.D. log IC_{50})[a]	Viral resistance (*n*-fold)	IC_{50} (S.D. log IC_{50})	Viral resistance (*n*-fold)	IC_{50} (S.D. log IC_{50})	Viral resistance (*n*-fold)
Ala	740.1 (0.103)	20.0	9.91 (0.216)	0.9	6.36 (0.135)	1.5
Cys	985.8 (0.121)	26.7	11.16 (0.250)	1.0	4.74 (0.038)	1.1
Asp	>10,000	>200	309.0 (0.057)	28.8	2.62 (0.060)	0.6
Glu	>10,000	>200	366.0 (0.132)	34.1	4.90 (0.064)	1.2
Phe	2105 (0.086)	57.0	20.81 (0.096)	1.9	2.87 (0.119)	0.7
Gly	5258 (0.061)	142.3	31.41 (0.075)	2.9	2.78 (0.025)	0.7
His	435.6 (0.072)	11.8	16.90 (0.072)	1.6	5.67 (0.039)	1.4
Ile	70.22 (0.059)	1.9	9.66 (0.089)	0.9	2.49 (0.068)	0.6
Lys	2556 (0.090)	69.2	50.16 (0.126)	4.7	5.67 (0.094)	1.4
Leu	74.59 (0.040)	2.0	9.48 (0.088)	0.9	6.24 (0.055)	1.5
Met	272.9 (0.079)	7.4	19.20 (0.065)	1.8	6.89 (0.043)	1.7
Asn	1868 (0.098)	50.5	26.78 (0.040)	2.5	5.51 (0.047)	1.3
Pro	8118 (0.167)	219.6	45.39 (0.126)	4.2	3.74 (0.817)	0.9
Gln	4849 (0.053)	131.2	41.64 (0.113)	3.9	6.81 (0.053)	1.6
Arg	3961 (0.090)	107.2	57.43 (0.087)	5.4	5.46 (0.062)	1.3
Ser	1147 (0.054)	31.0	26.29 (0.086)	2.5	5.95 (0.038)	1.4
Thr	325.3 (0.053)	8.8	18.62 (0.106)	1.7	3.68 (0.159)	0.9
Trp	1637 (0.108)	44.3	23.65 (0.062)	2.2	2.62 (0.055)	0.6
Tyr	4073 (0.076)	110.2	34.62 (0.085)	3.2	3.34 (0.054)	0.8
Val (WT)	36.96 (0.032)	1.0	10.73 (0.061)	1.0	4.15 (0.074)	1.0

[a] S.D. are given over the Log IC_{50}, as the method used to calculate the IC_{50} uses a logarithmic scale on the *x* axis.

TABLE 2

Summary of physicochemical analysis

N36(L6)C34 peptide	$-[\theta]_{222\ nm}$	% Helicity at 10 μM	T_m at 10 μM[a]	M_{obs}/M_{calc}[b]
	10^3 *degree·cm²·dmol⁻¹*		°C	
Ala	34.1	100	69	3.1
Cys	32.3	95	74	3.1
Asp	21.7	64	58	3.2
Glu	29.7	87	68	3.1
Phe	31.6	93	72	3.1
Gly	32.2	95	67	3.1
His	31.8	94	70	3.1
Ile	32.5	96	80	3.1
Lys	27.5	81	73	3.2
Leu	32.9	97	73	3.0
Met	34.0	100	73	3.0
Asn	29.1	86	67	3.0
Pro	29.5	87	60	3.1
Gln	32.4	95	71	3.0
Arg	29.0	85	72	3.0
Ser	33.4	98	65	3.0
Thr	31.7	93	76	3.0
Trp	32.9	97	73	3.1
Tyr	32.0	94	72	3.0
Val (WT)	34.5	100	80	3.0

[a] All CD scans and melts were performed with 10 μM peptide solutions in phosphate-buffered saline (pH 7.0). The midpoint of thermal denaturation (T_m) was calculated from the thermal dependence of the CD signal at 222 nm.

[b] M_{obs}/M_{calc} is the apparent molecular mass determined from sedimentation equilibrium data divided by the expected mass of a monomer.

wavelength dependence pattern shown in Fig. 3*A*. Most variants showed a similar pattern, indicating an α-helical content of >90% (Fig. 3*A*; Table 2). A number of amino acid substitutions decreased the α-helical content to <90% (V38E/K/N/P/R), whereas the V38D substitution reduced the α-helicity most dramatically (to 64%). The reduced helix content of the V38P six-helix bundle can be easily explained by the helix-breaking properties of this amino acid, and it is likely that the primary effect of the substitution is on the helix content of HR1. This effect may explain why V38P causes resistance to T20 and T1249. The reduced α-helicity of other substitutions is less easily explained. For example, Glu is extremely well accommodated in α-helices (59–61), but the V38E six-helix bundle nevertheless showed reduced α-helicity. A plausible explanation is that the V38E substitution does not directly affect the α-helix content of HR1 but indirectly affects that of HR2, possibly interfering with proper packing of HR2 with HR1. Similar effects may occur for V38K/N/P/R. These findings are also relevant for the drug-HR1 interactions and have implications for the observed resistance (see below).

The thermal stability of the variant six-helix bundles was determined by monitoring the CD signal at 222 nm over a temperature range. The midpoints of thermal denaturation (T_m) are given in Table 2, and selected denaturation curves are shown in Fig. 3*B*. Under these conditions, the T_m of the WT peptide was 80 °C, whereas the T_m of the mutants ranged from 58 to 80 °C. Almost all substitutions destabilized the six-helix bundle to some extent, with the V38A/D/E/G/P/S substitutions causing the largest effects (>10 °C drop in T_m). Not surprisingly, substitutions that reduced α-helicity often caused a decrease in thermal stability (*e.g.* for V38D/E/N/P, less evident for V38K/R). However, the small amino acids Ala/Gly/Ser caused a profound reduction of thermal stability (T_m 65–69) but without a noticeable effect on the helix content (95–100%). Taken together these results indicate that substitutions at position 38 of gp41 can lead to a substantial reduction of α-helical content and destabilization of the six-helix bundle.

Energetics of Drug-HR1 Interactions—Resistance to HIV-1 inhibitors is often caused by mutations that lower the affinity of the target for the drug. Many common resistance mutations to HIV-1 reverse transcriptase and protease inhibitors exemplify this type of resistance (62–64), and a similar mechanism of resistance has been proposed for T20 resistance mutations at position 38 (65). An important contributor to drug affinity is the energy that is released upon binding of the drug (binding energy). The binding energy is composed of energy loss, caused among other things by the decrease in entropy, and energy gain, caused by the acquisition of drug-target contacts. We studied the binding energies of the 20 HR1 variants with the three gen-

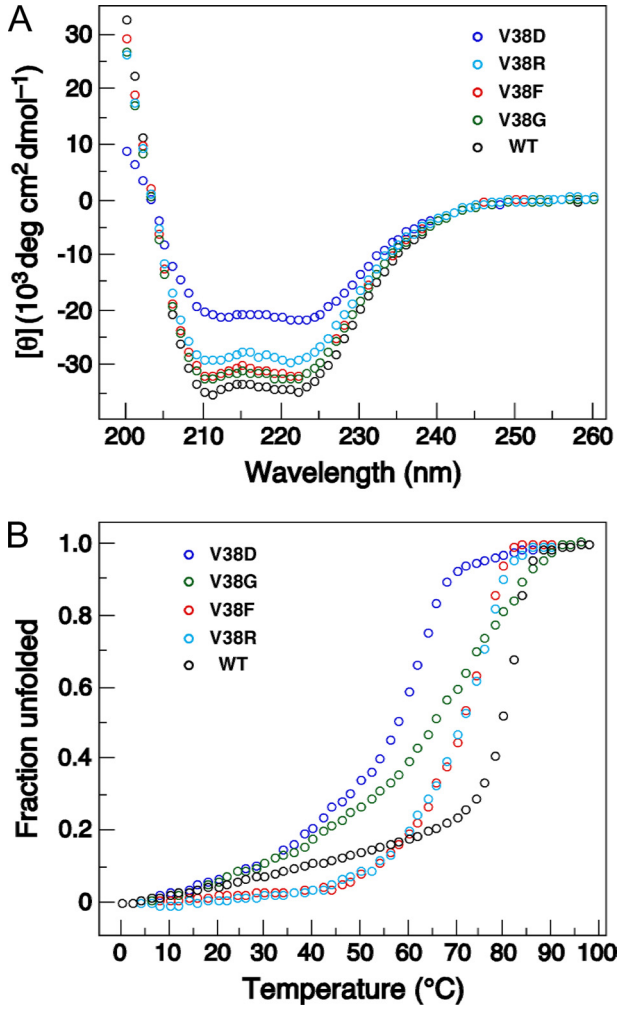

FIGURE 3. **Circular dichroism data for the wild-type and mutant six-helix bundle complexes V38D/F/G/R/W.** *A*, circular dichroism spectra at 10 mM peptide concentration in phosphate-buffered saline (pH 7.0) at 4 °C. *B*, temperature dependence of molar ellipticity at 222 nm in phosphate-buffered saline (pH 7.0) at 10 mM peptide concentration. The increase in the fraction of unfolded molecules is shown as a function of temperature.

erations of peptide inhibitors *in silico*. Models of the T20-HR1, T1249-HR1, and T2635-HR1 complexes were generated based on the core structure of gp41 and the binding energies of the 60 complexes were calculated using HADDOCK2.0. We found a correlation between the calculated binding energy and the thermal stability of the six-helix bundle observed in our biophysical experiments ($p = 0.0024$; data not shown). A higher calculated binding energy corresponds with a higher thermal stability. This provided confidence in the *in silico* analyses on the energetics of the drug-HR1 interactions. HR1 in complex with T20, T1249, and T2635 revealed binding energies of 160, 208, and 254 kcal mol^{-1}, respectively, consistent with the escalating inhibitory capacities of the three generations of inhibitors (Fig. 4).

We next investigated the binding energies of T20 with the 20 HR1 variants. Comparable binding energies were observed for V38C/F/H/I/K/L/M/P/T/W/Y (150–167 kcal mol^{-1}, Fig. 4, supplemental Table S1), whereas V38A/D/E/G/N/Q/R/S caused a substantial decrease (binding energies <150 kcal mol^{-1}). Interestingly, all aromatic residues showed higher binding energy than WT. Correlation and regression analysis showed a trend between the binding energy and sensitivity to T20 ($p = 0.035$; data not shown). An increased resistance to T20 correlated with a lower binding energy of T20 to HR1. However, the aromatic residues did not fit this trend.

We were intrigued by the anomalous binding energies of the aromatic amino acids. One would expect that the bulky aromatic rings would disturb the interactions with T20, causing a decrease in binding energy that would explain the observed resistance. Surprisingly, we found an increased binding energy for the aromatic residues Phe and Trp and only a small decrease for Tyr. A potential explanation could lie in the methodology. The calculations of the binding energies were based on T20-HR1 complexes in which the 38 side chains are accommodated optimally within the complex as a result of the optimization process during the modeling. The aromatic rings can be accommodated very well in the T20-HR2 complex after refinement, but it is highly unlikely that when T20 docks onto HR1, the 38 side chain is in this minimized "ideal" conformation. On the contrary, the aromatic side chains may stick out and obstruct proper T20 docking and/or binding, which would explain the observed resistance. We, therefore, constructed an additional model of T20 in complex with the V38F mutant and forced the aromatic side chain in a conformation that protrudes from the HR1 surface (F2; Fig. 4 and supplemental Table S2). The binding energy based on this complex was indeed lower (152.7 *versus* 166.0 kcal mol^{-1} for T20 binding).

The binding energies of the set of HR1 mutants with T1249 and T2635 ranged from 187 to 223 and 232 to 260 kcal mol^{-1}, respectively, and this variation was similar to the T20-HR1 complexes (~30 kcal mol^{-1}; Fig. 4 and supplemental Table S1). Furthermore, the trends observed were similar. Thus, the amino acids that caused decreased binding energies for T20 mostly had similar effects on the binding energies for T1249 and T2635. However, despite these similarities, we could not observe a correlation between the T1249-HR1 and T2635-HR1 binding energies and resistance, as we had seen with T20. A likely explanation is the overall higher binding energy of the former two inhibitors and a relatively decreased contribution of residue 38 to the drug-HR1 binding energy. Thus, T1249 may be less dependent and T2635 not dependent on the contribution of residue 38 to the overall binding energy.

Effect of Charge Interactions—Strikingly, charged residues at position 38 caused the highest resistance to T20, and charged residues could confer resistance to T1249 but not to T2635. Further inspection of the peptide-HR1 interface revealed that residue 38 of gp41 interacts with residues Gln-142, Asn-145, Glu-146, and Leu-149 in HR2 or the inhibitor (Fig. 5, *A–D*). The presence of Glu-146 in HR2 may explain why charged residues at position 38 cause an effect on six-helix bundle helix content and resistance. The electrostatic repulsion by Glu-146 in T20 and T1249 readily explains why V38D/E causes resistance. The resistance of V38K/R is counterintuitive, but it appears that formation of a salt bridge between V38K/R and Glu-146 is incompatible with packing of HR2/T20/T1249 onto HR1 as exemplified by the decreased helical content and lower six-helix bundle stability (Fig. 3, Table 2). Glu-146 is also present in T2635. However, in T2635 Glu-146 is involved in an intramo-

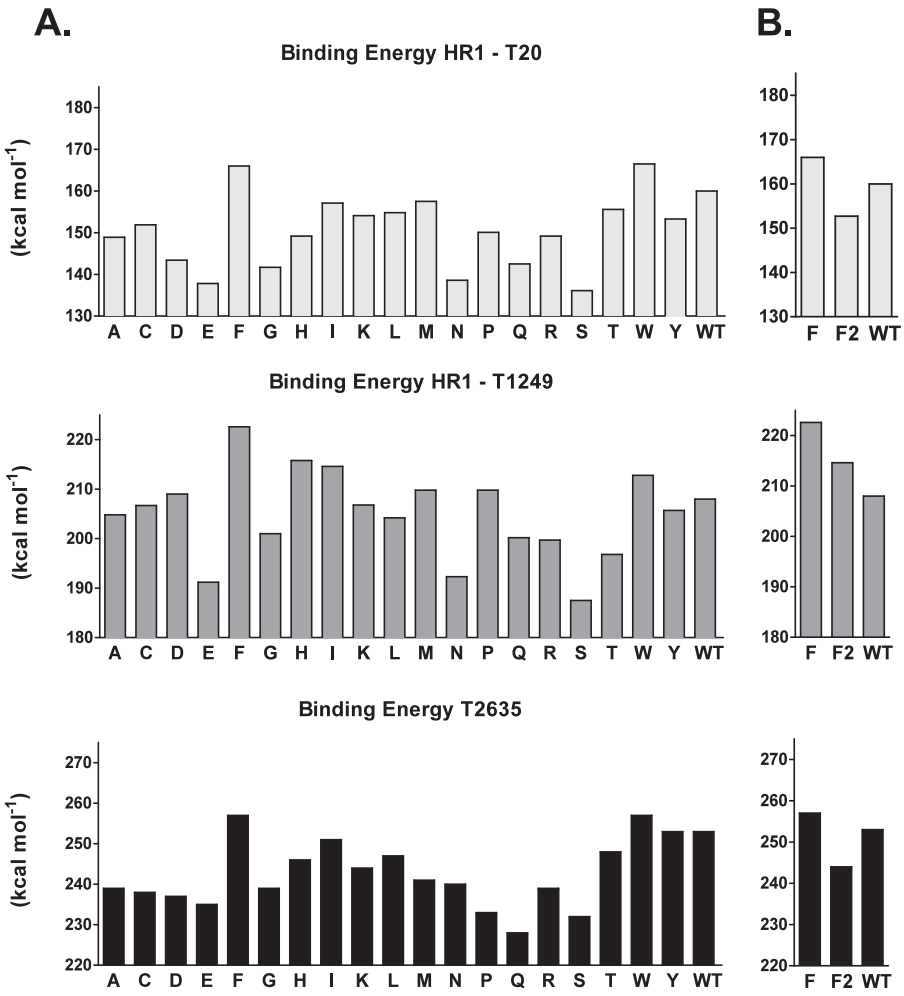

FIGURE 4. **Calculated binding energy for the three peptide inhibitors to the HR1 trimer core containing mutations at position 38 (*A panels*) and for V38F in two different conformations (*B panels*).**

lecular salt bridge with Arg-150 as part of the design to stabilize the helical structure of the peptide (27). This resulting neutral net charge may explain why even the charged residues at position 38 do not cause resistance to T2635 (Figs. 5*C* and 6).

To verify this possibility, we introduced this salt bridge in T1249 and removed it from T2635. Thus, we introduced Q150R in T1249 to pair with Glu-146 ($T1249^{mut}$, Figs. 1 and 5*D*), and we removed the specific salt bridge from T2635 by the reverse R150Q change, resulting in exposure of the charged Glu-146 ($T2635^{mut}$). We then performed single cycle infection experiments in the absence and presence of these variant peptides and determined the IC_{50} for WT and mutants containing a charged residue at position 38 (V38D/E/K/R) (Fig. 5, *E* and *F*, Table 3). The IC_{50} for $T1249^{mut}$ for WT virus was slightly decreased compared with the parental T1249 (2-fold), consistent with the helix-stabilizing effect of the salt bridge (27). Conversely, the removal of the salt bridge from T2635 caused a minor IC_{50} increase. Importantly, the Arg substitution in $T1249^{mut}$ almost completely abrogated the resistance caused by the charged residues at position 38 (from up to 40-fold to only 4-fold), confirming the hypothesis that electrostatic interactions of Glu-146 with charged residues at position 38 (negative or positive) are responsible for the resistance. We did not observe significant resistance differences between T2635 and $T2635^{mut}$. Apparently, the total binding energy of the T2635-HR1 interaction is high enough to accommodate even an electrostatic clash between Glu-146 and V38D/E. There are two alternative explanations why T2635 could be less sensitive to mutations at position 38. First, the binding site of T2635 on the HR1 trimer is different. The T2635 binding site overlaps for a large part with those of T20 and T1249 but is shifted three helical turns. Therefore, position 38 binds close to the C terminus of T2635, and this may not be the energetic core of the binding site. Second, T2635 is a stabilized helix that may not depend on the same type of docking as T20 and T1249; the latter two have to fold onto the hydrophobic groove of the HR1 trimer to acquire their helical structure. T2635 already has a preformed, large contact surface that may have a different docking mechanism that is less easy to escape from. This will be further addressed in the discussion.

DISCUSSION

Mutation of position 38 in HIV-1 gp41 can induce resistance to T20 and T1249, both *in vivo* and *in vitro*. Here, we have determined the impact of all 20 amino acids at this gp41 position for the sensitivity against three generations of peptide fusion inhibitors: T20, T1249, and T2635. In addition, we have collected biophysical and computational data on these gp41 variants. Combined, these data provide detailed insight into the underlying mechanisms of fusion inhibitor resistance.

Estimated Binding Energy Versus Docking

We found a weak correlation between increased T20 resistance and decreased binding energy of the T20-HR1 complex. Thus, the binding energy can only in part explain the resistance profiles of the 38 variants. For T1249 and T2635 the resistance cannot readily be explained by the variations in binding energy. It is, therefore, likely that residue 38 does not only contribute to the binding energy but is important for the initial docking of the peptides onto HR1. Indeed, it has been described that the LLSGIV stretch (residues 32–38 of gp41) is a critical docking site for T20 (66), and this may also explain the critical role of position 38 in resistance development.

If residue 38 is essential for binding/docking of T20, one would expect it to be crucial for the HR2 interaction as well as T20 and HR2 are similar in sequence. Indeed, we found a cor-

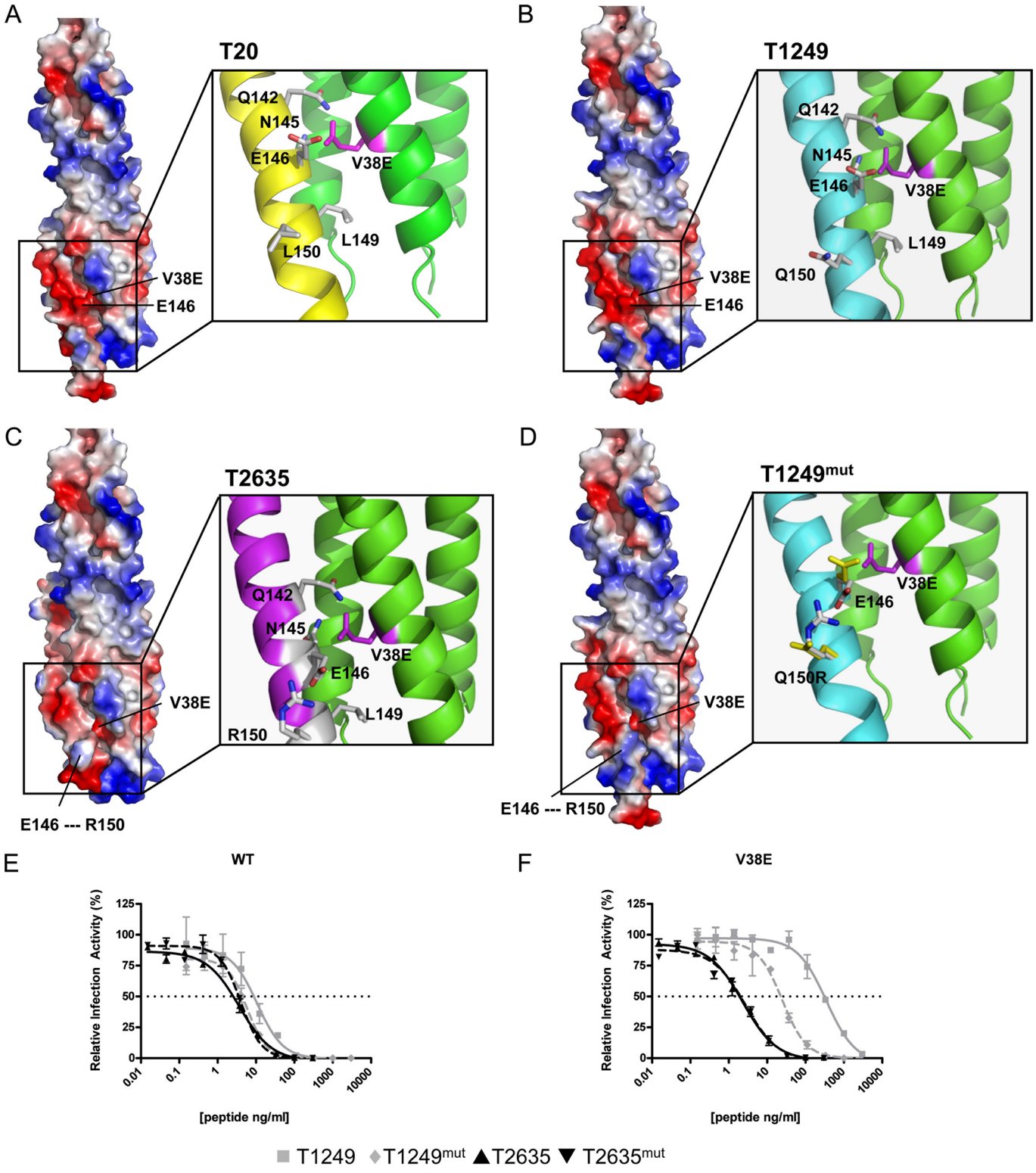

FIGURE 5. **Neutralization of an exposed charge at position 146 in the drug restores drug inhibition.** Contacts between T20 (*A*), T1249 (*B*), T2635 (*C*), and T1249^{mut} (*D*) and the HR1 trimer are shown. The electrostatic potentials were mapped on the surface of peptides and HR1 separately. The *boxed region* is also shown as a *ribbon drawing with sticks* representation for the side chains important for the interaction with position 38 (Gln-142, Asn-145, Glu-146, and Leu-149, Leu-150/Gln-150/Arg-150; *underlined* in the HR2 sequence shown in Fig. 1). The clashing charges of V38E in HR1 and Glu-146 in T20 and T1249 are apparent in *panels A* and *B*. The intramolecular salt bridge between Glu-146 and Arg-150 in T2635 (*C*) and T1249^{mut} (*D*) neutralizes the negative charge at Glu-146. The conformation of residues Glu-146 and Gln-150 in T1249 are represented in the structure of T1249^{mut} (*D*) in *yellow* for comparison. Inhibition of WT (*E*) and V38E (*F*) virus by T1249, T2635, T1249^{mut}, and T2635^{mut}. See supplemental Fig. S2 for the graphs of mutants V38D, V38K, and V38R.

relation between T20-HR1 binding energy and six-helix bundle stability ($p = 0.0042$), and we observed dramatic effects on six-helix bundle formation and infectivity with some substitutions. However, it should be noted that HR2 may be less dependent on such an initial docking event as it is already tethered to HR1 via the gp41 loop domain. Therefore, resistance mutations may

TABLE 3
Effect of charged amino acids in peptide fusion inhibitors

Variant	T1249		$T1249^{mut}$		T2635		$T2635^{mut}$	
	IC_{50} (S.D. log IC_{50})[a]	Viral resistance (*n*-fold)	IC_{50} (S.D. log IC_{50})[a]	Viral resistance (*n*-fold)	IC_{50} (S.D. log IC_{50})[a]	Viral resistance (*n*-fold)	IC_{50} (S.D. log IC_{50})[a]	Viral resistance (*n*-fold)
Asp (−)	439.4 (0.166)	41.2	22.72 (0.061)	3.9	1.52 (0.038)	0.5	2.20 (0.058)	0.6
Glu (−)	348.0 (0.089)	32.6	24.94 (0.061)	4.2	2.33 (0.042)	0.8	2.76 (0.067)	0.7
Lys (+)	57.97 (0.062)	5.4	6.93 (0.046)	1.2	3.29 (0.103)	1.2	5.44 (0.146)	1.5
Arg (+)	51.26 (0.264)	4.8	15.24 (0.054)	2.6	3.85 (0.123)	1.4	4.70 (0.100)	1.3
Val	10.67 (0.094)	1.0	5.879 (0.041)	1.0	2.83 (0.074)	1.0	3.69 (0.035)	1.0

[a] Values, presented in ng/ml, were calculated as described under "Experimental Procedures." Results shown are derived from experiments performed in duplicate and are representative of at least three independent experiments. Inhibition curves of single cycle infection experiments can be found in Fig. 5*B* and supplemental Fig. S2.

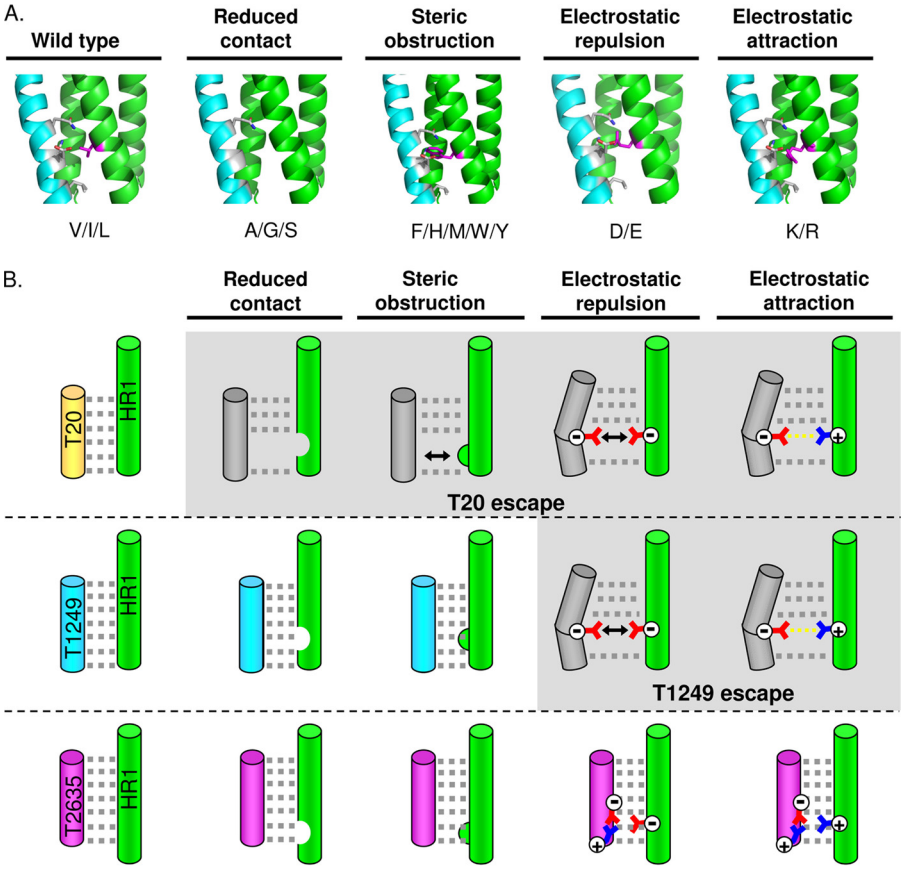

FIGURE 6. **Four mechanisms of resistance to fusion inhibitors.** Molecular models (*A*) and schematic representation (*B*) of four different mechanisms of fusion inhibitor resistance. Small amino acids (Ala/Gly/Ser) create a hole in the contact site, whereas large residues (Phe/His/Met/Trp/Tyr) form a bulk that causes steric repulsion. Negatively charged residues (Asp/Glu) cause electrostatic repulsion, whereas positively charged amino acids (Lys/Arg) can form a salt bridge with the inhibitory peptide, possibly causing non-optimal helix packing and/or docking.

have a more dramatic impact on the T20-HR1 interaction than on the HR2-HR1 interaction, and this is exactly a scenario that viruses would prefer for the selection of drug resistance mutations.

The increase in total binding energy of T2635-HR1 and to a lesser extent T1249-HR1 may explain why these drugs are less dependent on residue 38. The relative contribution of this single residue to the total binding energy is decreased. Another issue that may be taken into account is the level of structure of the drugs in solution. T20 exists predominantly as a random coil (~12% helix content) and needs the docking onto the HR1 coiled coil to acquire an α-helical structure, whereas T1249 is ~50% helical in solution. T2635 was specifically designed to be more stable (~75% helix content and a T_m of 86 °C in complex with HR1 compared with 59 °C for T1249 and <5 °C for T20) and, therefore, may be less dependent on the initial docking event to obtain its structure (27, 67).

Because the binding site of T1249 and T2635 is shifted compared with that of T20, their binding and/or docking may be more dependent on a hydrophobic pocket which is located near the C-terminal end of the HR1 coiled coil (68). The pocket binding domain, which is absent in T20, may contribute to the enhanced binding energy for T1249 and T2635 observed in our *in silico* analysis. We note that the binding of a lipid binding domain at the C terminus of T20 is absent in our analysis (68–70). This may constitute an underestimation of the binding energy for T20.

Mechanisms of Resistance

From our results, we can deduce four well defined mechanisms of resistance to fusion inhibitors (excluding the resistance of V38P that probably causes a kink in HR1) (Fig. 6).

Reduced Contact—Small amino acids such as Ala/Gly/Ser at position 38 are smaller than the WT Val, creating a "gap" in the binding site for T20. This reduces the number of contacts between HR1 and T20, resulting in a lower binding energy and resistance (Fig. 6). Obviously, the same should be the case for the HR2-HR1 interaction. Indeed we observed dramatically reduced six-helix bundle stability despite the fact that A/G did not alter six-helix bundle formation itself (as indicated for example by the high α-helix content).

Steric Obstruction—The opposite effect is induced by large residues Phe/His/Met/Trp/Tyr that create a "bulge," which sterically hinders the attachment of T20 to HR1. Although these larger residues can be accommodated quite well in the six-helix bundle complex (as indicated by high helix content, considerable six-helix bundle stability, relatively high infectivity, and large binding energies for T20), they probably affect the initial docking of T20 onto HR1.

These two types of resistance mechanisms suggest that there is a correlation between the size of an amino acid at position 38 and resistance to T20. We indeed observed such a trend (data not shown), although it was not significant. Both small and large amino acid caused resistance to T20, whereas intermediate sized amino acids displayed T20 sensitivity (Val/Ile/Leu). Several amino acids did not fit this trend. In particular, the charged amino acids behaved differently, which calls for alternative resistance mechanisms.

Electrostatic Repulsion—A third type of resistance proposed for negatively charged residues is electrostatic repulsion (Asp/Glu). This is facilitated by the juxtaposition of a negatively charged residue (Glu-146) in HR2, T20, and T1249. The presence of a negative charge at position 38 caused a decrease in α-helical content, six-helix bundle stability, and T20-HR1 binding energy. Despite the fact that amino acids like Asp and especially Glu, are well accommodated in α-helices (60, 61), a large decrease in helical content is observed. This suggests that these amino acids do not disturb the formation of the HR1 helix but affect the HR2 helix. This explains the high level of resistance to T20 and the resistance to T1249. The structural design of the T2635 peptide reveals why this peptide is not repulsed by the negative HR1 charge. In the design of T2635, this Glu-146 residue is specifically placed in a helix stabilizing salt bridge, resulting in a net neutral charge in that area of the peptide (Fig. 5*C*). To directly test this scenario, we paired the negative charge of T1249 in an intramolecular salt bridge ($T1249^{mut}$), which reduced the resistance profile of the V38D/E mutants dramatically.

Electrostatic Attraction—Interestingly, positive charges also resulted in resistance to both T20 and T1249. We do not have an entirely satisfying explanation for this, but the potential formation of a salt bridge between Arg/Lys and Glu-146 may not be accommodated in a configuration that is compatible with the proper T20-HR1 or HR2-HR1 packing (as confirmed by a reduced helicity and stability of the six-helix bundle). The introduction of a positive charge affects the electrostatic potential and might result in improper steering of the components when docking. Although a salt bridge might form, this is probably not compatible with an optimal HR1-peptide interface.

Other common T20 and T1249 resistance mutations identified *in vitro* and *in vivo* are G36D/E and N43D/K, representing changes from neutral to negative and positive charges (29, 30, 35, 71–73) that may influence the HR1-peptide interaction in a similar fashion as V38D/E/K/R. Residue 43 in HR1 is in close contact with residues Glu-137 in HR2 or peptide inhibitors (74). We studied the binding energies of G36D, V38D, and N43D HR1 variants with the three generations of peptide inhibitors *in silico* (supplemental Fig. S3 and Table S1). G36D, V38D, and N43D caused a decrease in binding energy of T20 corresponding with the observed resistance (29, 30, 32). N43D, but not G36D and V38D, caused a decrease in binding energy of T1249, confirming that binding energy is not the only determinant for sensitivity to T1249. All three HR1 variants displayed decreased binding energy with T2635, but the differences are relatively small when the total binding energy is taken into account. Thus, the resistance mechanisms we describe are likely to apply to other positions than 38 as well.

Implications for the Design of Novel Antiviral Fusion Inhibitors

We can make two important recommendations for the design of novel peptide fusion inhibitors. First, we give indications for the relative minimal binding energy that is required for potent inhibition and that may prevent easy viral escape by a single mutation in the binding site. To prevent a single substitution in the binding site from causing resistance, the binding energy for the peptide-target interaction, which can be computed from the six-helix bundle structure, should be high such that a single mutation only causes a relatively small change in the overall binding energy. We cannot give absolute values as our calculated binding energies are only an approximation and different methods might lead to different estimates. An additional advantage of such a mutation-tolerant mechanism of inhibition is that more natural virus variants will display sensitivity to the drug. The accumulation of multiple resistance mutations may provide resistance but will require more time (75) and will likely have a more dramatic effect on viral fitness.

Second, our data suggest that the presence of exposed charges on the peptide at the drug-target interface, unless involved in an intramolecular salt bridge, are not desirable as it provides the virus with an easy possibility to generate the most powerful mechanism of resistance; that is, electrostatic repulsion. These findings may guide the design of novel fusion inhibitors targeting viruses with class I fusion proteins.

Acknowledgments—We are grateful to Ilja Bontjer and Stef Heynen for technical assistance.

REFERENCES

1. Harrison, S. C. (2008) *Nat. Struct. Mol. Biol.* **15,** 690–698
2. Kielian, M., and Rey, F. A. (2006) *Nat. Rev. Microbiol.* **4,** 67–76
3. Melikyan, G. B. (2008) *Retrovirology* **5,** 111
4. Decroly, E., Vandenbranden, M., Ruysschaert, J. M., Cogniaux, J., Jacob, G. S., Howard, S. C., Marshall, G., Kompelli, A., Basak, A., and Jean, F. (1994) *J. Biol. Chem.* **269,** 12240–12247
5. Hallenberger, S., Bosch, V., Angliker, H., Shaw, E., Klenk, H. D., and Garten, W. (1992) *Nature* **360,** 358–361
6. Trkola, A., Purtscher, M., Muster, T., Ballaun, C., Buchacher, A., Sullivan, N., Srinivasan, K., Sodroski, J., Moore, J. P., and Katinger, H. (1996) *J. Virol.* **70,** 1100–1108
7. Wu, L., Gerard, N. P., Wyatt, R., Choe, H., Parolin, C., Ruffing, N., Borsetti, A., Cardoso, A. A., Desjardin, E., Newman, W., Gerard, C., and Sodroski, J. (1996) *Nature* **384,** 179–183
8. Chan, D. C., Fass, D., Berger, J. M., and Kim, P. S. (1997) *Cell* **89,** 263–273
9. Cladera, J., Martin, I., Ruysschaert, J. M., and O'Shea, P. (1999) *J. Biol. Chem.* **274,** 29951–29959
10. Jacobs, A., Garg, H., Viard, M., Raviv, Y., Puri, A., and Blumenthal, R. (2008) *Vaccine* **26,** 3026–3035
11. Jones, P. L., Korte, T., and Blumenthal, R. (1998) *J. Biol. Chem.* **273,** 404–409
12. Weissenhorn, W., Dessen, A., Harrison, S. C., Skehel, J. J., and Wiley, D. C. (1997) *Nature* **387,** 426–430
13. Bosch, B. J., Martina, B. E., Van Der Zee, R., Lepault, J., Haijema, B. J., Versluis, C., Heck, A. J., De Groot, R., Osterhaus, A. D., and Rottier, P. J. (2004) *Proc. Natl. Acad. Sci. U.S.A.* **101,** 8455–8460
14. Ou, W., and Silver, J. (2005) *J. Virol.* **79,** 4782–4792
15. Porotto, M., Carta, P., Deng, Y., Kellogg, G. E., Whitt, M., Lu, M., Mungall, B. A., and Moscona, A. (2007) *J. Virol.* **81,** 10567–10574
16. Wang, E., Sun, X., Qian, Y., Zhao, L., Tien, P., and Gao, G. F. (2003) *Biochem. Biophys. Res. Commun.* **302,** 469–475
17. Zhu, J., Jiang, X., Liu, Y., Tien, P., and Gao, G. F. (2005) *J. Mol. Biol.* **354,**

601–613
18. Wild, C., Greenwell, T., and Matthews, T. (1993) *AIDS Res. Hum. Retroviruses* **9,** 1051–1053
19. Wild, C., Greenwell, T., Shugars, D., Rimsky-Clarke, L., and Matthews, T. (1995) *AIDS Res. Hum. Retroviruses* **11,** 323–325
20. Wild, C., Oas, T., McDanal, C., Bolognesi, D., and Matthews, T. (1992) *Proc. Natl. Acad. Sci. U.S.A.* **89,** 10537–10541
21. Wild, C. T., Shugars, D. C., Greenwell, T. K., McDanal, C. B., and Matthews, T. J. (1994) *Proc. Natl. Acad. Sci. U.S.A.* **91,** 9770–9774
22. Chinnadurai, R., Münch, J., and Kirchhoff, F. (2005) *AIDS* **19,** 1401–1405
23. Eron, J. J., Gulick, R. M., Bartlett, J. A., Merigan, T., Arduino, R., Kilby, J. M., Yangco, B., Diers, A., Drobnes, C., DeMasi, R., Greenberg, M., Melby, T., Raskino, C., Rusnak, P., Zhang, Y., Spence, R., and Miralles, G. D. (2004) *J. Infect. Dis.* **189,** 1075–1083
24. Lalezari, J. P., Bellos, N. C., Sathasivam, K., Richmond, G. J., Cohen, C. J., Myers, R. A., Jr., Henry, D. H., Raskino, C., Melby, T., Murchison, H., Zhang, Y., Spence, R., Greenberg, M. L., Demasi, R. A., and Miralles, G. D. (2005) *J. Infect. Dis.* **191,** 1155–1163
25. Menzo, S., Castagna, A., Monachetti, A., Hasson, H., Danise, A., Carini, E., Bagnarelli, P., Lazzarin, A., and Clementi, M. (2004) *New Microbiol.* **27,** 51–61
26. He, Y., Xiao, Y., Song, H., Liang, Q., Ju, D., Chen, X., Lu, H., Jing, W., Jiang, S., and Zhang, L. (2008) *J. Biol. Chem.* **283,** 11126–11134
27. Dwyer, J. J., Wilson, K. L., Davison, D. K., Freel, S. A., Seedorff, J. E., Wring, S. A., Tvermoes, N. A., Matthews, T. J., Greenberg, M. L., and Delmedico, M. K. (2007) *Proc. Natl. Acad. Sci. U.S.A.* **104,** 12772–12777
28. Aquaro, S., D'Arrigo, R., Svicher, V., Perri, G. D., Caputo, S. L., Visco-Comandini, U., Santoro, M., Bertoli, A., Mazzotta, F., Bonora, S., Tozzi, V., Bellagamba, R., Zaccarelli, M., Narciso, P., Antinori, A., and Perno, C. F. (2006) *J. Antimicrob. Chemother.* **58,** 714–722
29. Melby, T., Sista, P., DeMasi, R., Kirkland, T., Roberts, N., Salgo, M., Heilek-Snyder, G., Cammack, N., Matthews, T. J., and Greenberg, M. L. (2006) *AIDS Res. Hum. Retroviruses* **22,** 375–385
30. Mink, M., Mosier, S. M., Janumpalli, S., Davison, D., Jin, L., Melby, T., Sista, P., Erickson, J., Lambert, D., Stanfield-Oakley, S. A., Salgo, M., Cammack, N., Matthews, T., and Greenberg, M. L. (2005) *J. Virol.* **79,** 12447–12454
31. Rimsky, L. T., Shugars, D. C., and Matthews, T. J. (1998) *J. Virol.* **72,** 986–993
32. Wei, X., Decker, J. M., Liu, H., Zhang, Z., Arani, R. B., Kilby, J. M., Saag, M. S., Wu, X., Shaw, G. M., and Kappes, J. C. (2002) *Antimicrob. Agents Chemother.* **46,** 1896–1905
33. Baldwin, C. E., Sanders, R. W., Deng, Y., Jurriaans, S., Lange, J. M., Lu, M., and Berkhout, B. (2004) *J. Virol.* **78,** 12428–12437
34. Chinnadurai, R., Rajan, D., Münch, J., and Kirchhoff, F. (2007) *J. Virol.* **81,** 6563–6572
35. Eggink, D., Baldwin, C. E., Deng, Y., Langedijk, J. P., Lu, M., Sanders, R. W., and Berkhout, B. (2008) *J. Virol.* **82,** 6678–6688
36. Melby, T., Demasi, R., Cammack, N., Miralles, G. D., and Greenberg, M. L. (2007) *AIDS Res. Hum. Retroviruses* **23,** 1366–1373
37. Peden, K., Emerman, M., and Montagnier, L. (1991) *Virology* **185,** 661–672
38. Sanders, R. W., Busser, E., Moore, J. P., Lu, M., and Berkhout, B. (2004) *AIDS Res. Hum. Retroviruses* **20,** 742–749
39. Das, A. T., Klaver, B., and Berkhout, B. (1999) *J. Virol.* **73,** 81–91
40. Jeeninga, R. E., Hoogenkamp, M., Armand-Ugon, M., de Baar, M., Verhoef, K., and Berkhout, B. (2000) *J. Virol.* **74,** 3740–3751
41. Derdeyn, C. A., Decker, J. M., Sfakianos, J. N., Wu, X., O'Brien, W. A., Ratner, L., Kappes, J. C., Shaw, G. M., and Hunter, E. (2000) *J. Virol.* **74,** 8358–8367
42. Guex, N., and Peitsch, M. C. (1997) *Electrophoresis* **18,** 2714–2723
43. Peitsch, M. C. (1996) *Biochem. Soc. Trans.* **24,** 274–279
44. Hooft, R. W., Vriend, G., Sander, C., and Abola, E. E. (1996) *Nature* **381,** 272
45. de Vries, S. J., van Dijk, A. D., Krzeminski, M., van Dijk, M., Thureau, A., Hsu, V., Wassenaar, T., and Bonvin, A. M. (2007) *Proteins* **69,** 726–733
46. Dominguez, C., Boelens, R., and Bonvin, A. M. (2003) *J. Am. Chem. Soc.* **125,** 1731–1737
47. Jorgensen, W. L., and Tirado-Rives, J. (1988) *J. Am. Chem. Soc.* **110,** 1657–1666
48. Fernández-Recio, J., Totrov, M., and Abagyan, R. (2004) *J. Mol. Biol.* **335,** 843–865
49. Lu, M., Ji, H., and Shen, S. (1999) *J. Virol.* **73,** 4433–4438
50. Sanders, R. W., Vesanen, M., Schuelke, N., Master, A., Schiffner, L., Kalyanaraman, R., Paluch, M., Berkhout, B., Maddon, P. J., Olson, W. C., Lu, M., and Moore, J. P. (2002) *J. Virol.* **76,** 8875–8889
51. Kunkel, T. A. (1985) *Proc. Natl. Acad. Sci. U.S.A.* **82,** 488–492
52. Edelhoch, H., Brand, L., and Wilchek, M. (1967) *Biochemistry* **6,** 547–559
53. Chen, Y. H., Yang, J. T., and Chau, K. H. (1974) *Biochemistry* **13,** 3350–3359
54. Cantor, C., and Schimmel, P. (1980) *Biophysical Chemistry,* Part III, pp. 1131–1132, W. H. Freeman and Co., New York
55. Shu, W., Ji, H., and Lu, M. (1999) *Biochemistry* **38,** 5378–5385
56. Laue, T. M., Shah, B. D., Ridgeway, T. M., Pelletier, S. L., Harding, S. E., Rowe, A. J., and Horton, J. C. (1992) in *Analytical Ultracentrifugation in Biochemistry and Polymer Science*, pp. 90–125, Royal Society of Chemistry, Cambridge, England
57. Sanders, R. W., Korber, B., Lu, M., Berkhout, B., and Moore, J. P. (2002) in *HIV Sequence Compendium 2002* (Kuiken, C., Foley, B., Freed, E., Hahn, B., Marx, P., McCutchan, F., Mellors, J., and Wolinsky, S., eds) pp. 43–68, Theoretical Biology and Biophysics Group, Los Alamos National Laboratory, Los Alamos, New Mexico
58. Lu, M., Stoller, M. O., Wang, S., Liu, J., Fagan, M. B., and Nunberg, J. H. (2001) *J. Virol.* **75,** 11146–11156
59. Chou, P. Y., and Fasman, G. D. (1974) *Biochemistry* **13,** 222–245
60. Chou, P. Y., and Fasman, G. D. (1974) *Biochemistry* **13,** 211–222
61. Levitt, M. (1978) *Biochemistry* **17,** 4277–4285
62. Boyer, P. L., and Hughes, S. H. (1995) *Antimicrob. Agents Chemother.* **39,** 1624–1628
63. Diallo, K., Götte, M., and Wainberg, M. A. (2003) *Antimicrob. Agents Chemother.* **47,** 3377–3383
64. Mahalingam, B., Louis, J. M., Reed, C. C., Adomat, J. M., Krouse, J., Wang, Y. F., Harrison, R. W., and Weber, I. T. (1999) *Eur. J. Biochem.* **263,** 238–245
65. Steger, H. K., and Root, M. J. (2006) *J. Biol. Chem.* **281,** 25813–25821
66. Trivedi, V. D., Cheng, S. F., Wu, C. W., Karthikeyan, R., Chen, C. J., and Chang, D. K. (2003) *Protein Eng.* **16,** 311–317
67. Martins Do Canto, A. M., Palace Carvalho, A. J., Prates Ramalho, J. P., and Loura, L. M. (2008) *J. Pept. Sci.* **14,** 442–447
68. Liu, S., Jing, W., Cheung, B., Lu, H., Sun, J., Yan, X., Niu, J., Farmar, J., Wu, S., and Jiang, S. (2007) *J. Biol. Chem.* **282,** 9612–9620
69. Caffrey, M., Cai, M., Kaufman, J., Stahl, S. J., Wingfield, P. T., Covell, D. G., Gronenborn, A. M., and Clore, G. M. (1998) *EMBO J.* **17,** 4572–4584
70. Caffrey, M., Cai, M., Kaufman, J., Stahl, S. J., Wingfield, P. T., Gronenborn, A. M., and Clore, G. M. (1997) *J. Mol. Biol.* **271,** 819–826
71. Greenberg, M. L., and Cammack, N. (2004) *J. Antimicrob. Chemother.* **54,** 333–340
72. Sista, P. R., Melby, T., Davison, D., Jin, L., Mosier, S., Mink, M., Nelson, E. L., DeMasi, R., Cammack, N., Salgo, M. P., Matthews, T. J., and Greenberg, M. L. (2004) *AIDS* **18,** 1787–1794
73. Xu, L., Pozniak, A., Wildfire, A., Stanfield-Oakley, S. A., Mosier, S. M., Ratcliffe, D., Workman, J., Joall, A., Myers, R., Smit, E., Cane, P. A., Greenberg, M. L., and Pillay, D. (2005) *Antimicrob. Agents Chemother.* **49,** 1113–1119
74. Bai, X., Wilson, K. L., Seedorff, J. E., Ahrens, D., Green, J., Davison, D. K., Jin, L., Stanfield-Oakley, S. A., Mosier, S. M., Melby, T. E., Cammack, N., Wang, Z., Greenberg, M. L., and Dwyer, J. J. (2008) *Biochemistry* **47,** 6662–6670
75. Keulen, W., Boucher, C., and Berkhout, B. (1996) *Antiviral Res.* **31,** 45–57

Detailed Mechanistic Insights into HIV-1 Sensitivity to Three Generations of Fusion Inhibitors

Dirk Eggink, Johannes P. M. Langedijk, Alexandre M. J. J. Bonvin, Yiqun Deng, Min Lu, Ben Berkhout and Rogier W. Sanders

J. Biol. Chem. 2009, 284:26941-26950.
doi: 10.1074/jbc.M109.004416 originally published online July 17, 2009
